Featuring work from Dr Hiroo Hata from the Research Institute of Science for Safety and Sustainability at the National Institute of Advanced Industrial Science and Technology (AIST), Japan.

Kinetic study of isoprene hydroxy hydroperoxide radicals reacting with sulphur dioxide and their global-scale impact on sulphate formation

The rate constants of isoprene-derived organic peroxide radicals reacting with sulphur dioxide were estimated by the microcanonical kinetic calculations, and their global-scale impacts on sulphate formation were considered.

As featured in:

See Hiroo Hata and Kenichi Tonokura, *Environ. Sci.: Processes Impacts*, 2024, **26**, 1147.

ROYAL SOCIETY OF CHEMISTRY

rsc.li/espi

Registered charity number: 207890

Environmental Science Processes & Impacts

ROYAL SOCIETY OF CHEMISTRY

PAPER

View Article Online
View Journal | View Issue

Cite this: *Environ. Sci.: Processes Impacts*, 2024, **26**, 1147

Kinetic study of isoprene hydroxy hydroperoxide radicals reacting with sulphur dioxide and their global-scale impact on sulphate formation†

Hiroo Hata *[a] and Kenichi Tonokura [b]

Isoprene is the most relevant volatile organic compound emitted during the biosynthesis of metabolism processes. The oxidation of isoprene by a hydroxy radical (OH) is one of the main consumption schemes that generate six isomers of isoprene hydroxy hydroperoxide radicals (ISOPOOs). In this study, the rate constants of ISOPOOs + sulphur dioxide (SO_2) reactions that eventually generate sulphur trioxide (SO_3), the precursor of sulphate aerosol (SO_4^{2-}(p)), are determined using microcanonical kinetic theories coupled with molecular structures and energies estimated by quantum chemical calculations. The results show that the reaction rates range from 10^{-27} to 10^{-20} cm^3 $molecule^{-1}$ s^{-1}, depending on the atmospheric temperature and structure of the six ISOPOO isomers. The effect of SO_3 formation from SO_2 oxidation by ISOPOOs on the atmosphere is evaluated by a global chemical transport model, along with the rate constants obtained from microcanonical kinetic theories. The results show that SO_3 formation is enhanced in regions with high SO_2 or low nitrogen oxide (NO), such as China, the Middle East, and Amazon rainforests. However, the production rates of SO_3 formation by ISOPOOs + SO_2 reactions are eight orders of magnitude lower than that from the OH + SO_2 reaction. This is indicative of SO_4^{2-}(p) formation from the direct oxidation of SO_2 by ISOPOOs, which is almost negligible in the atmosphere. The results of this study entail a detailed analysis of SO_3 formation from gas-phase reactions of isoprene-derived products.

Received 25th April 2024
Accepted 21st May 2024

DOI: 10.1039/d4em00232f

rsc.li/espi

Environmental significance

This study discusses the impact of six isomers of isoprene hydroxy hydroperoxide radicals (ISOPOOs) on the global-scale formation of sulphate aerosol (SO_4^{2-}(p)). The rate constants of ISOPOOs + SO_2 and subsequent reactions are estimated using microcanonical kinetic theory (transition-state theory and RRKM/Master equation theory) coupled with quantum chemical calculations. The obtained rate constants are incorporated into a global chemical transport model, GEOS-Chem, to evaluate the effects of ISOPOOs on sulphur trioxide (SO_3), a precursor of SO_4^{2-}(p). The obtained results suggest that the direct oxidation of SO_2 by ISOPOOs contributes maximally 10^{-6} % of gas-phase SO_3 formation in the high-isoprene regions, indicating the negligible contribution of ISOPOOs to the direct oxidation of SO_2 for forming SO_4^{2-}(p) on a global scale.

Introduction

Isoprene (C_5H_8) is a biogenic volatile organic compound (BVOC) emitted to the atmosphere during the biosynthesis of metabolic processes.[1–3] Isoprene contains two carbon–carbon double bonds, and its reactivity enables the high-production potential of tropospheric ozone (O_3) and secondary organic aerosol (SOA).[4,5] Globally, isoprene dominates ~60% of the total VOC emissions that are condensed in forests and vegetated areas such as the Amazon.[6–8]

Fig. S1 of the ESI† shows typical pathways for the oxidation of isoprene by O_3 and hydroxy radical (OH).[9] The oxidation of isoprene by O_3, shown in Fig. S1(a),† produces Criegee intermediates (CIs) that finally form sulphate aerosols (SO_4^{2-}(p)) by the oxidation of sulphur dioxide (SO_2), the nuclei of particulate matter,[10–15] However, the contribution of the CIs-to-SO_4^{2-}(p) formation is negligible compared to that of OH.[9] Conversely, the oxidation of isoprene by OH forms six isomers of isoprene hydroxy hydroperoxide radicals (ISOPOOs) as shown in Fig. 1, which then form isoprene epoxydiols (IEPOXs) as shown in Fig. S1(b).†[16–19] Thereafter, owing to low volatility and the water-soluble chemical structure from the two hydroxyl groups of IEPOXs, SOA is eventually generated. Several studies have reported the importance of in-cloud oxidation of bisulphate (HSO_3^-) by the reaction of ISOPOOHs (formed by the hydroperoxyl radical (HO_2) + ISOPOOs reactions described in Fig. S1(b)†) to form SO_4^{2-}(p).[20–22]

[a]*Research Institute of Science for Safety and Sustainability, National Institute of Advanced Industrial Science and Technology (AIST), 16-1 Onogawa, Tsukuba, Ibaraki 305-8569, Japan. E-mail: hata-hiroo@aist.go.jp; Tel: +81-80-2212-2713*

[b]*Department of Environment Systems, Graduate School of Frontier Sciences, The University of Tokyo, Kashiwano-ha, Kashiwa, Chiba 277-8563, Japan*

† Electronic supplementary information (ESI) available. See DOI: https://doi.org/10.1039/d4em00232f

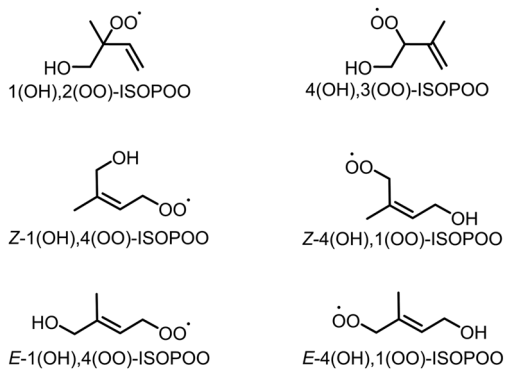

Fig. 1 Six structural isomers of isoprene hydroxy hydroperoxide radical (ISOPOO).

Notably, the formation pathways of SOA and SO_4^{2-} shown in Fig. S1(b) and (c)† can proceed under low NO conditions owing to the high reactivity of NO and HO_2 with organic peroxide radicals (RO_2) including ISOPOOs.[23–26] Some of the ISOPOOs hold ring structures formed by the intramolecular hydrogen bond of the hydroxy (–OH) and peroxyl radical (–OO) groups, which cause unimolecular isomerization due to hydrogen shift from –OH to –OO.[27,28] Wennberg *et al.* reviewed and summarized ISOPOO reactions,[29] with their pathways already considered in atmospheric chemical mechanisms. Unlike other atmospheric oxidants such as OH, nitrate radical (NO_3) or RO_2 including ISOPOOs are relatively stable in the atmosphere and can accumulate to high concentrations in oxidation systems.[30] Thus, to the best of our knowledge, limited studies have focused on the direct oxidation of SO_2 by ISOPOOs, with low expected rates of oxidation estimated by Kurtén *et al.* who conducted the theoretical calculation of the reaction of SO_2 with four peroxide radicals; HO_2, methyl peroxide (CH_3OO), ethyl peroxide (C_2H_5OO) and hydroxymethyl peroxide ($CH_3(OH)OO$).[31] Nevertheless, isoprene is the most relevant BVOC in the atmosphere, and owing to the high global concentrations of isoprene and isoprene-derived intermediates, acknowledgement of the contributions of ISOPOOs to the oxidation and formation of SO_2 and SO_4^{2-}(p), respectively, is significant.

In this study, the direct oxidation rate constants of SO_2 obtained from the six isomers of ISOPOOs, shown in Fig. 1 (1(OH),2(OO)-ISOPOO, 4(OH),3(OO)-ISOPOO, *Z*-1(OH),4(OO)-ISOPOO, *Z*-4(OH),1(OO)-ISOPOO, *E*-1(OH),4(OO)-ISOPOO, and *E*-4(OH),1(OO)-ISOPOO), are determined using the transition state theory. The estimated rate constants are incorporated into the chemical mechanism of the global chemical transport model to evaluate the effect of SO_2 oxidation by ISOPOOs on the global scale SO_3 formation. The results of this study are expected to contribute towards a quantitative understanding of direct oxidation of SO_2 by ISOPOOs in the atmosphere.

Methodology

Kinetic analysis

Quantum chemical calculations. This study focused on the rate constants of the six isomers of ISOPOOs, shown in Fig. 1, which reacted with SO_2. The reactions produced sulphur trioxide (SO_3, the precursor of SO_4^{2-}(p)) and alkoxyl radicals derived from ISOPOOs (ISOPOs). Additionally, the reactions generate intermediate products described as $ISOPOOSO_2$s, in which the lone pair of –OO adducted to the unoccupied orbital of the sulphur atom in SO_2. For simplicity, the descriptions of the functional groups of ISOPOOs and $ISOPOOSO_2$s were abbreviated, such that 1(OH),2(OO)-ISOPOO and *E*-1(OH),4(OO)-$ISOPOOSO_2$ were described as 1,2-ISOPOO and *E*-1,4-$ISOPOOSO_2$, respectively. Gaussian 16 (G16; rev. C.01) was used for quantum chemical calculations to study the potential energy surface (PES) of the reactions.[32] The M06-2X level of density functional theory (DFT)[33] was applied to optimise the chemical structure of the components and obtain rovibrational properties and zero-point vibrational energies. Considering that there are several internal rotations for the targeted species of this study, we chose to focus on the global-energetically minimized structures for data accruement. Single-point electronic energies for all the optimised structures were calculated using the couple cluster method (CCSD(T)).[34] Dunning's triple-zeta basis function was applied to both DFT and single-point energy calculations. Previous studies revealed that the importance of extra-tight *d* functions should be considered for the DFT and CCSD(T) calculations of molecules that contain sulphur to be uniformly efficient with correct energy values.[35–38] Therefore, herein, two Dunning's triple-zeta functions, aug-cc-pVTZ and aug-cc-p(V+d)Z,[39] were applied to the DFT and CCSD(T) calculations to verify the effect of the extra-tight *d* function on the energy level of sulphur-containing molecules. T_1-diagnostic was also applied to the CCSD(T) calculations to check the multireference character of the molecules.[40] The calculated results for the TS structures were validated using intrinsic reaction coordinate calculations[41] at the same level of theory (M06-2X/aug-cc-pVTZ and M06-2X/aug-cc-pV(T+*d*)Z). Stability analysis was conducted for all the open-shell calculations of radical species. As per the results of this observation, all structures were stable. The vibrational frequencies were scaled by 0.946, while the zero-point vibrational energies were scaled by 0.971.[42]

Calculation of rate constants using transition-state theory. The rate constants of the reactions that hold relevant, vibrationally adiabatic energy barriers (zero-point corrected energy barrier) were calculated using the transition-state theory (TST)[43] with the Gaussian post-processor (GPOP).[44] To briefly summarize TST, the high-pressure limit rate constant of a specific reaction in a thermodynamically stable environment, k_{TST}, could be formulated as eqn (1).

$$k_{TST} = \frac{k_B T}{h} \frac{Q^{\#}(T)}{Q(T)} \exp\left(-\frac{E_0}{k_B T}\right) \quad (1)$$

where h is the Planck constant (J s), k_B is the Boltzmann constant (J K^{-1}), T is the ambient temperature (K), Q is the total partition function of the reactants, $Q^{\#}$ is the partition function of the TS, and E_0 is the vibrationally adiabatic energy barrier (J). The partition functions Q and $Q^{\#}$ were the products of partition functions of four physical properties: translation of molecules, molecular vibration, moment of inertia of molecular rotation,

and electronic state. These parameters were obtained from the quantum chemical calculations as aforementioned, while GPOP automatically read the results of the G16 output files to derive Q and $Q^{\#}$. Eckart's tunnelling correction[45] was applied to the TST calculations.

Evaluation of branching ratio calculated by RRKM/ME theory. Unimolecular decomposition reactions exhibited pressure dependence, which resulted in a microcanonical non-equilibrium state of the reactants and TS, leading to errors in the rate constants evaluated by the TST. Such local-non-equilibrium kinetics were evaluated using the Rice–Ramsperger–Kassel–Marcus (RRKM)/Master Equation (ME) theory.[46] Briefly, the RRKM/ME theory was summarised to express the non-equilibrium reactions of unimolecular decompositions caused by the collision of reactants with bath gases such as nitrogen (N_2) and oxygen (O_2), following the commonly applied ME expressed as eqn (2).

$$\frac{dN_i}{dt} = [\mathrm{M}]\sum_{j=0}^{n}\left(k_{ij}N_j - k_{ji}N_i\right) - k_{\mathrm{uni},i}N_i \quad (2)$$

where N_i is the number of energy states i ($\Sigma N_i = 1$), M represents the bath gas (N_2 and O_2 in ambient), k_{ij} is the rate of transition from energy state j to i, and $k_{\mathrm{uni},i}$ is the microcanonical unimolecular decomposition rate constant at energy state i. $k_{\mathrm{uni},i}$ was determined using RRKM theoretical calculations. In this study, RRKM/ME calculations were conducted using a steady-state unimolecular master-equation solver (SSUMES).[47] Troe's bi-exponential collisional energy transfer model was applied to the evaluated intermediates of SSUMES.[48] Collision relaxation energy transfer ($\langle\Delta E\rangle_{\mathrm{down}}$) of 130 cm^{-1} between the reactants and M was chosen according to a previous study, where the value was determined by measuring the relaxation energy of toluene relaxed by N_2.[49] Lennard–Jones collisional parameter, ε_K = 750 K and σ = 3.86 Å, were determined according to the potential well-depth of two 1,2-ISOPOOSO$_2$s calculated using G16 with the theory of M06-2X/aug-cc-pV(T+*d*)Z. The obtained potential curve was analysed, as shown in Fig. S2.† Eckart's tunnelling correction[45] was applied to the $k_{\mathrm{uni},I}$ calculations.

Global chemical transport modelling

The Goddard Earth observing system chemistry model (GEOS-Chem (v14.2.3))[50] was used to evaluate the global impact of the reactions between ISOPOOs and SO_2. For this study, a grid resolution of 2 × 2.5° (latitude × longitude) with 72 vertical layers holding the ground surface to the stratosphere was selected. The modern-era retrospective analysis for research and applications version 2 (MERRA2) was used as the meteorological input.[51] For emission inventories, emissions database for community emissions data system (CEDSv2) was used for anthropogenic emissions,[52] hemispheric transport of air pollution (HTAPv3) was used for ship emissions,[53] monthly-mean data of Aviation Emissions Inventory (AEIC2019) was used for aircraft emissions,[54] global fire emissions database (GFED) was used for biomass burning,[55] and the model of emissions of gases and aerosols from nature (MEGAN) was used for BVOC emissions.[56] The targeted period spanned from 1st July 2018 to 31st December 2019. The following six-month period was treated as a spin-off period, while the second year of 2019 was treated as the analysis term. The branching ratio and related reactions of the six isomers of ISOPOOs were modified using the full-chemistry module of the kinetic pre-processor (KPP) that controlled the chemical reactions of GEOS-Chem; the details are described in the subsequent section.

Results

Optimised structures and diagnostic values for the ISOPOO and SO_2 reactions

The globally optimised structures of the six ISOPOO isomers are shown in Fig. S3† and the detailed cartesian coordinates are listed in Tables S1 to S6 of the ESI.† Compounds 1,2-, 4,3-, *Z*-1,4- and *Z*-4,1-ISOPOOs adopted a ring structure due to the formation of intramolecular hydrogen bonds between –OH and –OO. *E*-1,4-ISOPOO also formed a ring structure, but the distance between –OH and –OO was large, enabling SO_2 to form a complex with *E*-1,4-ISOPOO, as shown in Fig. S4 and Tables S7 and S8 of the ESI.† *E*-4,1-ISOPOO had a straight chain structure. Peeters *et al.* conducted the optimization and energetical calculations of the six isomers of ISOPOOs using quantum chemical calculations (CCSD(T)/aug-cc-pVTZ//M06-2X/6-311++G(3df,2p)).[57] The obtained optimized structures of ISOPOOs well represented the results obtained by Peeters *et al.* The initial reactions of ISOPOOs + SO_2 led to intermediate products of ISOPOOSO$_2$s through the transition states of TS1, followed by the unimolecular decomposition of ISOPOOSO$_2$s to form SO_3 and alkoxy radicals (ISOPOs). The calculated structures of TS1 and TS2, ISOPOOs, ISOPOs, SO_2 and SO_3 are presented in Fig. S5 to S9 and Tables S9 to S34 of the ESI,† respectively.

Evaluation of the extra-tight *d* function of sulphur-containing molecules

Table 1 shows the total atomization energy (TAE) and zero-point energy (ZPE) of aug-cc-pVTZ and aug-cc-pV(T+*d*)Z obtained by M06-2X and CCSD(T) calculations. The values of the vibrational frequencies, rotational constants, electronic state and point group, spin contamination and T_1-diagnostic for the targeted molecules are listed in Tables S35–S48, S49–S50, S51, S52–S55 and S56–S57†respectively. For all species, the calculations that applied a basis set with extra-tight *d* functions showed a ~10 kcal mol^{-1} decrease in the TAE compared to the values for a normal basis set. Contrarily, all ZPE values obtained from the results of the extra-tight *d* function were ~0.1 to 0.2 kcal mol^{-1} higher than those of a normal basis-set. The reference TAE values of SO_2 and SO_3 were reported to be 258.3 and 343.7 kcal mol^{-1} respectively, and when compared to M06-2X and CCSD(T) for the two basis sets, the value of M06-2X was closer to the experimental results than that of CCSD(T). All the sulphur-included ISOPOO species demonstrated ~10 to 20 kcal mol^{-1} more stability when introducing the basis set encompassing the extra-tight *d* function. To the best of our knowledge, no experimental values of the TAE have been

Table 1 Total atomisation energies (kcal mol^{-1}) calculated by M06-2X/aug-cc-pVTZ (D_0), M06-2X/aug-cc-pV(T+*d*)Z (D_0_*d*), CCSD(T)/aug-cc-pVTZ (D_0) and CCSD(T)/aug-cc-pV(T+*d*)Z (D_0_*d*) and zero-point energies (kcal mol^{-1}) calculated by M06-2X/aug-cc-pVTZ (ZPE) and M06-2X/aug-cc-pV(T+*d*)Z (ZPE_*d*) for the sulphur-containing species targeted in this study. Diff indicates the difference between D_0_*d* and D_0 or between ZPE_*d* and ZPE

	M06-2X						CCSD(T)		
Molecule	D_0	D_0_*d*	Diff	ZPE	ZPE_*d*	Diff	D_0	D_0_*d*	Diff
SO_2	237.6	247.4	9.713	4.559	4.645	0.08597	231.5	240.4	8.896
SO_3	313.0	327.8	14.85	7.899	8.087	0.1883	302.7	316.8	14.07
1,2-TS1	1746	1756	10.14	92.61	92.70	0.08722	1705	1715	9.516
4,3-TS1	1745	1755	10.16	92.90	93.01	0.1086	1704	1713	9.528
E-1,4-TS1	1747	1757	9.896	93.41	93.47	0.06212	1705	1714	9.295
E-4,1-TS1	1744	1754	10.10	93.01	93.10	0.08346	1702	1711	9.468
Z-1,4-TS1	1745	1755	10.16	93.38	93.45	0.07216	1702	1712	9.542
Z-4,1-TS1	1744	1754	10.11	93.32	93.43	0.1117	1702	1711	9.475
1,2-ISOPOOSO$_2$	1749	1760	11.10	93.68	93.83	0.1569	1707	1718	10.69
4,3-ISOPOOSO$_2$	1747	1759	11.15	93.94	94.08	0.1450	1706	1716	10.75
E-1,4-ISOPOOSO$_2$	1750	1761	10.94	94.48	94.68	0.1958	1707	1718	10.57
E-4,1-ISOPOOSO$_2$	1746	1757	11.09	94.04	94.21	0.1688	1704	1715	10.70
Z-1,4-ISOPOOSO$_2$	1747	1759	11.07	94.35	94.54	0.1839	1705	1715	10.67
Z-4,1-ISOPOOSO$_2$	1747	1758	11.07	94.35	94.54	0.1945	1704	1715	10.67
1,2-TS2	1736	1749	12.44	92.29	92.47	0.1770	1698	1710	11.87
4,3-TS2	1736	1749	12.48	92.49	92.62	0.1299	1697	1709	11.90
E-1,4-TS2	1737	1750	12.31	92.74	92.90	0.1562	1697	1709	11.74
E-4,1-TS2	1720	1732	11.93	91.77	91.96	0.1945	1675	1685	10.02
Z-1,4-TS2	1737	1749	12.33	92.82	93.01	0.1908	1697	1708	11.75
Z-4,1-TS2	1734	1747	12.41	92.96	93.13	0.1719	1695	1707	11.79
E-1,4-complex1	1762	1771	9.467	93.37	93.39	0.02259	1720	1728	8.707
E-1,4-complex2	1779	1794	14.99	92.98	93.20	0.2115	1735	1749	14.31

reported for sulphur-containing ISOPOO species; therefore, it is hard to verify which basis sets are effective. Nevertheless, several studies have suggested the effectiveness of kinetic analyses that were conducted based on the basis-set results of the extra-tight *d* function (CCSD(T)/aug-cc-pV(T+*d*)Z//M06-2X/aug-cc-pV(T+*d*)Z).

Diagnostics of the electronic states of ISOPOO-related species

According to Tables S52–S55,† the open-shell radicals ($S = 0.5$) of the M06-2X calculations show almost no spin contamination after annihilation of the effect (the value could be $S(S+1) = 0.75$ when no spin contamination occurs). On the other hand, the CCSD(T) calculations exhibit weak spin contamination for the TS2 species. Additionally, only *E*-4,1-TS2 show the high value of 1.38 after annihilation. According to Tables S56 and S57 of the ESI,† all species with the exception of the TS2s meet the required T_1-diagnostic value for single-reference methods,[58] approximately ranging from less than 0.02 to 0.03. In terms of the TS2s apart from *E*-4,1-isomer shows a value lesser than 0.033, which meets the criterion of the T_1-diagnostic value for open-shell calculations,[58] and almost no multireference characteristic is expected. The results of the high-spin contamination and the high T_1-diagnostic value imply that *E*-4,1-TS2 has strong multireference characteristics and the single-point energy can be estimated by multireference wave function methods such as the Complete Active Space Second Order Perturbation Theory (CASPT2).[59] Nevertheless, further calculations were not conducted for *E*-4,1-TS2 in this study, because the total reaction rate of *E*-4,1-ISOPOO + SO_2 to form SO_3 and the total existence ratio of *E*-4,1-ISOPOO in the atmosphere were expected to be low, which is discussed in the later section. A detailed analysis of the multireference characteristics will be conducted as future work.

Potential energy diagram of the reaction of ISOPOO + SO_2

The potential energy diagram of the entire reaction initiated by 1,2-ISOPOO and SO_2 is shown in Fig. 2(a), and that by 4,3-, *Z*-1,4-, *Z*-4,1- and *E*-4,1-ISOPOOs are shown in Fig. S10 to S13 of the ESI.† According to Fig. 2(a) and S10 to S13,† the barrier heights for the formation of TS1 by ISOPOOs, barring *E*-1,4-ISOPOO, ranged from 7.9 to 9.1 kcal mol^{-1}. From Fig. 2(b), *E*-1,4-ISOPOO held a complex with SO_2, which stabilized the total energy of the reactant system to 14.0 kcal mol^{-1}. The barrier height from complex to TS1 rose to 12.7 kcal mol^{-1}. Thus, ISOPOOs, barring *E*-1,4-ISOPOO, reacted with SO_2; however, in terms of *E*-4,1-ISOPOO, the barrier height of TS2 was significantly higher than that of the other ISOPOOs, and less decomposition to SO_3 was expected. The barrier height of TS1 for the reaction of *E*-1,4-ISOPOO and SO_2 was ~4 kcal mol^{-1} higher than that of other ISOPOOs owing to the formation of the complex, and the reaction was expected to be very slow. The entire reaction was exothermic. Detailed kinetics are presented in the following section.

Results of kinetic calculations

Fig. 3 shows the rate constants calculated for the ISOPOOs + SO_2 reaction and the branching ratio (η) of ISOPOOSO$_2$s to form SO_3,

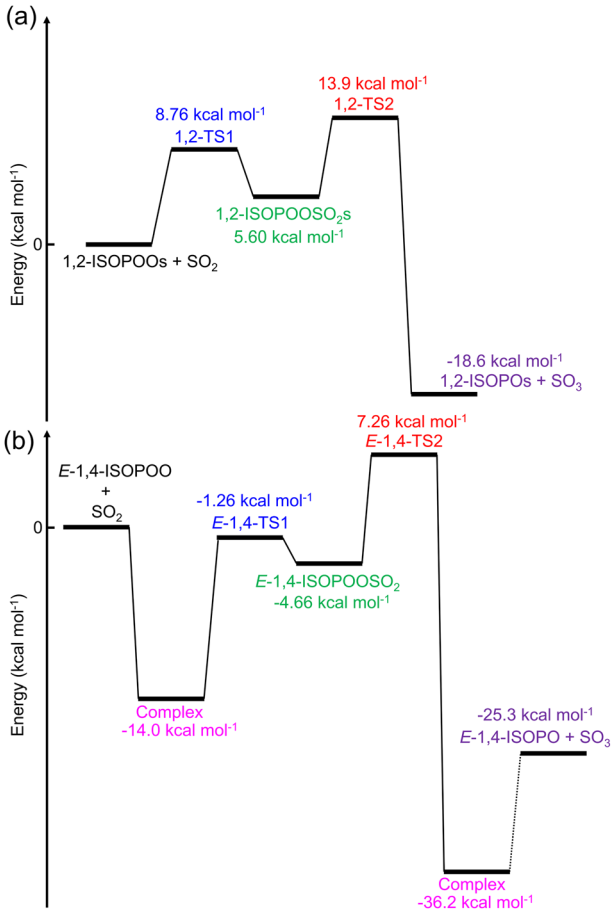

Fig. 2 Potential diagram of the entire ISOPOOs + SO_2 reaction obtained from the quantum chemical calculations for (a) 1,2-ISOPOO and (b) *E*-1,4-ISOPOO evaluated by CCSD(T)/aug-cc-pV(T+*d*)Z//M06-2X/aug-cc-pV(T+*d*)Z level of theory.

which were obtained by RRKM/ME calculation. The parameters of the rate constants in Arrhenius form are listed in Table S58 of the ESI.† *E*-1,4-ISOPOO showed 5 orders of lower magnitude for the SO_2 reaction at 298 K than that of other isomers, which ranged from $\sim 10^{-22}$ to 10^{-21} cm^3 molecule^{-1} s^{-1} in standard conditions ($T = 298$ K). Kurtén *et al.* suggested almost the same kinetic values, 5×10^{-21} cm^3 molecule^{-1} s^{-1} or less for the reactions of organic peroxides and SO_2 of which the value was consistent with the ISOPOOs results obtained in this study.[31] As aforementioned, the barrier height of the *E*-1,4-ISOPOO reacting with SO_2 was approximately 4 kcal mol^{-1} higher than that of the other isomers, leading to lower rate constants for the *E*-1,4-ISOPOO + SO_2 reaction. The branching ratios, η, required to form SO_3 by the unimolecular reactions of ISOPOOSO$_2$s, generated from ISOPOOs + SO_2 reactions, are described in parenthesis in Fig. 3. All the values of the unimolecular reactions were recorded at the conditions of 298 K and 1atm. The values of η, barring *E*-4,1-ISOPOO, ranged from $\sim$0.0005 to 0.009; thus, maximally only 1% of ISOPOOSO$_2$s decomposed to SO_3 and ISOPO, while the remaining ISOPOOSO$_2$s reproduced ISOPOO and SO_2 by a reverse reaction due to high energy barrier of TS2, as shown in Fig. 2. The value of η of *E*-4,1-ISOPOO was more than approximately 7 orders of magnitude lower than that of the other isomers, implying no complete generation of SO_3 from *E*-4,1-ISOPOO. Thus, both *E*-1,4- and *E*-4,1-ISOPOOs were less relevant to form SO_3 owing to the lower rate constant of the reaction with SO_2 for *E*-1,4-ISOPOO and lower η value for *E*-1,4-ISOPOO.

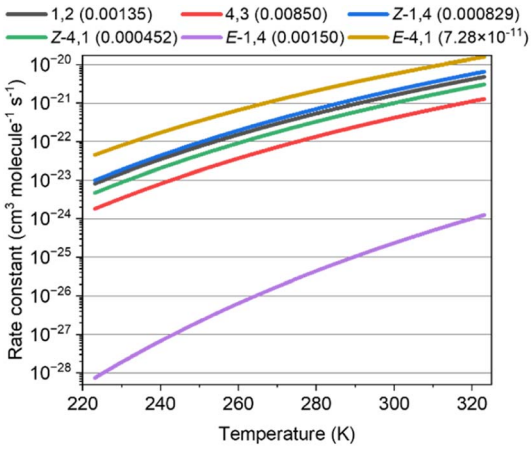

Fig. 3 Rate constants of the reaction of ISOPOOs + SO_2 to form ISOPOOSO$_2$s for six isomers of ISOPOO. The value inside the parenthesis indicates the branching ratio of unimolecular reactions of ISOPOOSO$_2$s to form SO_3.

Global-scale impact of ISOPOOs and SO_2 reactions on the formation of sulphates

Detail of the reaction mechanisms incorporated into the global chemical transport model

The impact of the ISOPOOs + SO_2 reactions on SO_3 formation was estimated using GEOS-Chem. Since the rate constants of the ISOPOOs + SO_2 reactions were low, direct incorporation of the kinetic parameters of these reactions resulted in reaching the limit of numerical error of GEOS-Chem. For this reason, we estimated the impact of the reactions *via* an indirect method, *i.e.*, by calculating the concentration of ISOPOOs and then multiplying the concentration of SO_2 by the rate constants in each grid to obtain the rate of SO_3 formation. For the estimations, the reactions related to *E*-1,4- and *E*-4,1-ISOPOOs were excluded because these two reactions were expected to be highly slower than the remaining reactions, according to the kinetic parameters described in Fig. 3. The reactions for the production of ISOPOOs from isoprene oxidation by OH were modified in this study. KPP defines ISOPOOs as IHOO1 and IHOO4, corresponding to 1(OH)–ISOPOOs and 4(OH)–ISOPOOs, which cannot be distinguished by the six geometric isomers shown in Fig. 1. In this study, IHOO1 and IHOO4 were divided into three isomers, each with a branching ratio as proposed in a previous study (1,2-ISOPOO: 0.479, 4,3-ISOPOO: 0.259, *Z*-1,4-ISOPOO: 0.049, *Z*-4,1-ISOPOO: 0.063, *E*-1,4-ISOPOO: 0.102, *E*-4,1-ISOPOO: 0.048).[29] All other IHOO1 and IHOO4-related reactions were substituted by the corresponding six geometric isomers.

Results of global chemical transport modelling

The annual mean tropospheric column concentrations of (a) total concentration of the six isomers of ISOPOO (molecule cm^{-2}), (b) rate of SO_3 formation from ISOPOOs + SO_2 reactions ($r_{ISOPOO\_SO_2} = \eta k_{ISOPOO\_SO_2}[ISOPOOs][SO_2]$ where η is the branching ratio of $ISOPOOSO_2$s to form SO_3 and $k_{ISOPOO\_SO_2}$ is the rate constant of ISOPOOs + SO_2 reactions; molecule cm^{-2} s^{-1}) and (c) ratio of the $r_{ISOPOO\_SO_2}$ to the rate of SO_3 formation from OH + SO_2 ($r_{OH\_SO_2}$) (%) are shown in Fig. 4. Here, OH was chosen to compare the rate of SO_2 oxidation because OH is the most relevant oxidiser of SO_2 in the atmosphere, which accounts for around 50% of total SO_2 oxidation.[9,60] The annual mean tropospheric column concentrations of isoprene, SO_2, NO and HO_2 are described in Fig. S14 to S17 of the ESI,† respectively. According to Fig. 4(a) and S14,† the distribution of ISOPOOs is condensed in high-isoprene regions such as the Amazon rainforests, Central Africa and Australia. On the other hand, according to Fig. 4(b), $r_{ISOPOO\_SO_2}$ is high not only in the high-isoprene regions, but also in highly polluted regions such as China, India, Middle Eastern regions and the north to middle regions of the American continent due to high SO_2 concentrations in those regions. Finally, according to Fig. 4(c), the ratio of $r_{ISOPOO\_SO_2}/r_{OH\_SO_2}$ is maximally $\sim 10^{-6}$% in the Amazon rainforests and Southeast Asian countries, which indicates that SO_3 formation from the ISOPOOs + SO_2 reactions is almost negligible, and that the reactions may not contribute to SO_4^{2-}(p) formation in the real atmosphere. The reason for the negligible contribution of the ISOPOOs + SO_2 reactions towards SO_3 formation is the low ISOPOOs concentrations caused by the scavengers of ISOPOOs such as NO, HO_2 and other organic peroxy radicals, and by the low-rate constants of entire reaction paths. Isoprene is the most popular VOC on a global scale, and ISOPOOs are the most relevant organic peroxy radicals generated from isoprene and OH reaction. However, according to the results of this study, the direct oxidation of SO_2 by ISOPOOs is almost negligible. This indicates that other organic peroxy radicals generated by the different VOCs may also not contribute to SO_3 and SO_4^{2-}(p) formations in the global-scale atmosphere.

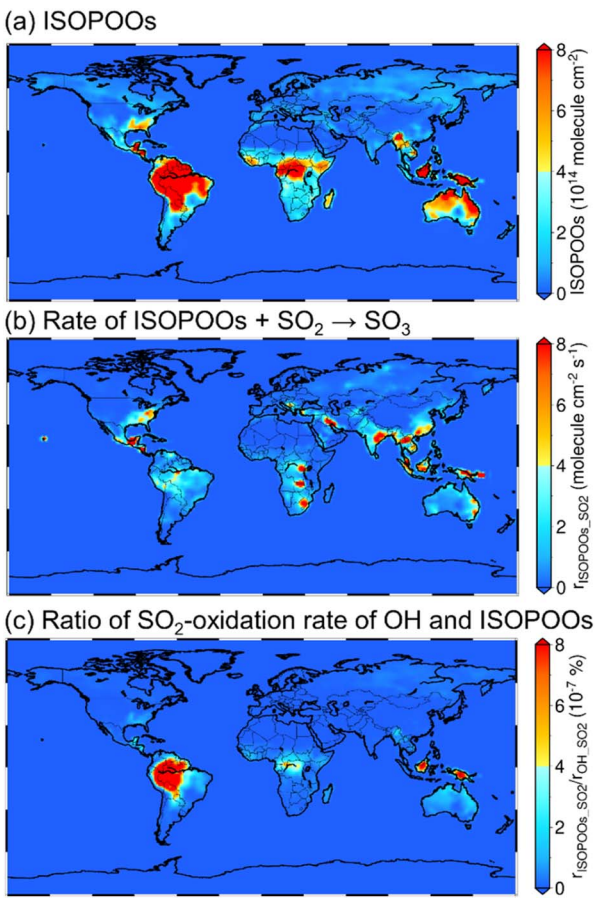

Fig. 4 Calculated results of the whole-year average of (a) total column-concentration of ISOPOOs, (b) rate of ISOPOOs + SO_2 reactions to form SO_3, and (c) ratio of the oxidation rate of SO_2 by ISOPOOs to the oxidation rate of SO_2 by OH.

Summary

The reaction kinetics of six isomers of ISOPOOs and SO_2 are evaluated using microcanonical kinetic calculations coupled with quantum chemical calculations. The results show that the reaction barriers of five isomers, 1,2-, 4,3-, *Z*-1,4-, *Z*-4,1- and *E*-4,1-ISOPOOs, are sufficient to form intermediate products, $ISOPOOSO_2$s, with rate constants ranging from $\sim 10^{-27}$ to $\sim 10^{-20}$ cm^3 $molecule^{-1}$ s^{-1}. The branching ratio of $ISOPOOSO_2$s to form SO_3 by unimolecular decomposition is estimated as maximally as 0.0085, implying the expected formulation of only a small amount of SO_3. Furthermore, the contribution of *E*-1,4- and *E*-4,1-ISOPOOs to sulphate aerosol formation is expected to be almost negligible owing to the low-rate constant of $ISOPOOSO_2$ (*E*-1,4-ISPOO) formation and the low branching ratio of SO_3 (*E*-4,1-ISOPOO) formation. The results of the global chemical transport modelling suggest that the rates of the ISOPOOs + SO_2 reactions are relatively higher in high-SO_2 and high-isoprene regions. Nevertheless, the contribution of the ISOPOOs + SO_2 reactions to form SO_3 was estimated to be eight orders of magnitude lower than that from the OH + SO_2 reactions, which indicated negligible effects of ISOPOOs to SO_4^{2-}(p) formation in the real atmosphere.

Author contributions

Hiroo Hata proposed the research concept, conducted kinetic analysis and global-chemical transport modelling, wrote the draft paper, and Kenichi Tonokura supervised and checked the work for accuracy.

Conflicts of interest

There are no conflicts to declare.

Acknowledgements

This study was supported by a Grant-in-Aid for Scientific Research (C) and (B) from the Japan Society for the Promotion of

Science (JSPS; Grant Number JP21K12286 and JP24K03088). We are grateful to the handling editor and the anonymous reviewers who raised suggestions and provided clarity to on behalf of this study.

References

1 T. D. Sharkey, A. E. Wiberley and A. R. Donohue, Isoprene emission from plants: why and how, *Ann. Bot.*, 2008, **101**, 5–18.
2 B. A. Logan, R. K. Monson and M. J. Potosnak, Biochemistry and physiology of foliar isoprene production, *Trends Plant Sci.*, 2000, **5**(11), 477–481.
3 L. Cappellin, F. Loreto, F. Biasioli, P. Pastore and K. McKinney, A mechanism for biogenic production and emission of MEK from MVK decoupled from isoprene biosynthesis, *Atmos. Chem. Phys.*, 2019, **19**, 3125–3135.
4 A. G. Carlton, C. Wiedinmyer and J. H. Kroll, A review of Secondary Organic Aerosol (SOA) formation from isoprene, *Atmos. Chem. Phys.*, 2009, **9**, 4987–5005.
5 J. C. Acosta Navarro, S. Smolander, H. Struthers, E. Zorita, A. M. Ekman, J. O. Kaplan, A. Guenther, A. Arneth and I. Riipinen, Global emissions of terpenoid VOCs from terrestrial vegetation in the last millennium, *J. Geophys. Res.: Atmos.*, 2014, **119**(11), 6867–6885.
6 K. Sindelarova, C. Granier, I. Bouarar, A. Guenther, S. Tilmes, T. Stavrakou, J.-F. Müller, U. Kuhn, P. Stefani and W. Knorr, Global data set of biogenic VOC emissions calculated by the MEGAN model over the last 30 years, *Atmos. Chem. Phys.*, 2014, **14**, 9317–9341.
7 R. von Kuhlmann, M. G. Lawrence, U. Pöschl and P. J. Crutzen, Sensitivities in global scale modeling of isoprene, *Atmos. Chem. Phys.*, 2004, **4**, 1–17.
8 E. V. Avzianova and P. A. Ariya, Temperature-dependent kinetic study for ozonolysis of selected tropospheric alkenes, *Int. J. Chem. Kinet.*, 2002, **34**(12), 678–684.
9 H. Hata, S. Hoshino, M. Fujita and K. Tonokura, Atmospheric impact of isoprene-derived Criegee intermediates and isoprene hydroxy hydroperoxide on sulfate aerosol formation in the Asian region, *Atmos. Environ.: X*, 2023, **20**, 100226.
10 G. T. Drozd, T. Kurtén, N. M. Donahue and M. I. Lester, Unimolecular decay of the dimethyl-substituted Criegee intermediate in alkene ozonolysis: decay time scales and the importance of tunneling, *J. Phys. Chem. A*, 2017, **121**(32), 6036–6045.
11 J. P. Hakala and N. M. Donahue, Pressure-dependent Criegee intermediate stabilization from alkene ozonolysis, *J. Phys. Chem. A*, 2016, **120**(14), 2173–2178.
12 M. J. Newland, A. R. Rickard, M. S. Alam, L. Vereecken, A. Muñoz, M. Ródenas and W. J. Bloss, Kinetics of stabilised Criegee intermediates derived from alkene ozonolysis: reactions with SO2, H2O and decomposition under boundary layer conditions, *Phys. Chem. Chem. Phys.*, 2015, **17**, 4076–4088.
13 M. J. Newland, B. S. Nelson, A. Muñoz, M. Ródenas, T. Vera, J. Tárrega and A. R. Rickard, Trends in stabilisation of Criegee intermediates from alkene ozonolysis, *Phys. Chem. Chem. Phys.*, 2020, **22**, 13698–13706.
14 A. R. Cox, M. Ammann, N. J. Crowley, H. Herrmann, E. M. Jenkin, F. V. McNeill, A. Mellouki, J. Troe and J. T. Wallington, Evaluated kinetic and photochemical data for atmospheric chemistry, *Atmos. Chem. Phys.*, 2020, **20**, 13497–13519.
15 H. K. Bates, D. J. Crounse, M. J. St. Clair, B. N. Bennett, B. T. Nguyen, H. J. Seinfeld, M. B. Stoltz and O. P. Wennberg, Gas phase production and loss of isoprene epoxydiols, *J. Phys. Chem. A*, 2014, **118**(7), 1237–1246.
16 S. H. Budisulistiorini, A. Nenes, A. G. Carlton, J. D. Surratt, V. F. McNeill and H. O. T. Pye, Simulating aqueous-phase isoprene-epoxydiol (IEPOX) secondary organic aerosol production during the 2013 Southern Oxidant and Aerosol Study (SOAS), *Environ. Sci. Technol.*, 2017, **51**(9), 5026–5034.
17 M. N. Chan, J. D. Surratt, M. Claeys, E. S. Edgerton, R. L. Tanner, S. L. Shaw, M. Zheng, E. M. Knipping, N. C. Eddingsaas, P. O. Wennberg and J. H. Seinfeld, Characterization and Quantification of isoprene-derived epoxydiols in ambient aerosol in the Southeastern United States, *Environ. Sci. Technol.*, 2010, **44**(12), 4590–4596.
18 T. B. Nguyen, M. M. Coggon, K. H. Bates, X. Zhang, R. H. Schwantes, K. A. Schilling, C. L. Loza, R. C. Flagan, P. O. Wennberg and J. H. Seinfeld, Organic aerosol formation from the reactive uptake of isoprene epoxydiols (IEPOX) onto non-acidified inorganic seeds, *Atmos. Chem. Phys.*, 2014, **14**, 3497–3510.
19 E. Dovrou, J. C. Rivera-Rios, K. H. Bates and F. N. Keutsch, Sulphate formation *via* cloud processing from isoprene hydroxyl hydroperoxides (ISOPOOH), *Environ. Sci. Technol.*, 2019, **53**, 12476–12484.
20 E. Dovrou, K. H. Bates, J. C. Rivera-Rios, J. L. Cox, J. D. Shutter and F. N. Keutsch, Towards a chemical mechanism of the oxidation of aqueous sulphur dioxide *via* isoprene hydroxyl hydroperoxides (ISOPOOH), *Atmos. Chem. Phys.*, 2021, **21**(11), 8999–9008.
21 T. Fang, P. S. J. Lakey, J. C. Rivera-Rios, F. N. Keutsch and M. Shiraiwa, Aqueous-phase decomposition of isoprene hydroxy hydroperoxide and hydroxyl radical formation by Fenton-like reactions with iron ions, *J. Phys. Chem. A*, 2020, **124**(25), 5230–5236.
22 A. P. Teng, J. D. Crounse and P. O. Wennberg, Isoprene peroxy radical dynamics, *J. Am. Chem. Soc.*, 2017, **139**(15), 5367–5377.
23 A. M. Miller, L. Y. Yeung, A. C. Kiep and M. J. Elrod, Overall rate constant measurements of the reactions of alkene-derived hydroxyalkylperoxy radicals with nitric oxide, *Phys. Chem. Chem. Phys.*, 2004, **6**, 3402–3407.
24 D. Zhang, R. Zhang and S. W. North, Experimental study of NO reaction with isoprene hydroxyalkyl peroxy radicals, *J. Phys. Chem. A*, 2003, **107**, 11013–11019.
25 P. Stevens, D. L'Esperance, B. Chuong and G. Martin, Measurements of the kinetics of the OH-initiated oxidation of isoprene: radical Propagation in the OH + isoprene + O_2 + NO reaction system, *Int. J. Chem. Kinet.*, 1999, **31**, 637–643.

26 D. Stone, L. K. Whalley and D. E. Heard, Tropospheric OH and HO2 radicals: field measurements and model comparisons, *Chem. Soc. Rev.*, 2012, **41**, 6348–6404.
27 G. da Silva, C. Graham and Z. F. Wang, Unimolecular β-hydroxyperoxy radical decomposition with OH recycling in the photochemical oxidation of isoprene, *Environ. Sci. Technol.*, 2010, **44**, 250–256.
28 M. E. Jenkin, J. C. Youg and A. R. Rickard, The MCM v3.3.1 degradation scheme for isoprene, *Atmos. Chem. Phys.*, 2015, **15**, 11433–11459.
29 P. O. Wennberg, K. H. Bates, J. D. Crounse, L. G. Dodson, R. C. McVay, L. A. Mertens, T. B. Nguyen, E. Praske, R. H. Schwantes, M. D. Smarte, J. M. St Clair, A. P. Teng, X. Zhang and J. H. Seinfeld, Gas-phase reactions of isoprene and its major oxidation products, *Chem. Rev.*, 2018, **118**, 3337–3390.
30 M. J. Goldman, W. H. Green and J. H. Kroll, Chemistry of simple organic peroxy radicals under atmospheric through combustion conditions: role of temperature, pressure, and NOx level, *J. Phys. Chem. A*, 2021, **125**(48), 10303–10314.
31 T. Kurtén, R. J. Lane, S. Jørgensen and G. H. Kjaergaard, A computational study of the oxidation of SO_2 to SO_3 by gas-phase organic oxidants, *J. Phys. Chem. A*, 2011, **115**(31), 8669–8681.
32 M. J. Frisch; G. W. Trucks; H. B. Schlegel; G. E. Scuseria; M. A. Robb; J. R. Cheeseman; G. Scalmani; V. Barone; G. A. Petersson; H. Nakatsuji; X. Li; M. Caricato; A. V. Marenich; J. Bloino; B. G. Janesko; R. Gomperts; B. Mennucci; H. P. Hratchian; J. V. Ortiz; A. F. Izmaylov; J. L. Sonnenberg; D. Williams-Young; F. Ding; F. Lipparini; F. Egidi; J. Goings; B. Peng; A. Petrone; T. Henderson; D. Ranasinghe; V. G. Zakrzewski; J. Gao; N. Rega; G. Zheng; W. Liang; M. Hada; M. Ehara; K. Toyota; R. Fukuda; J. Hasegawa; M. Ishida; T. Nakajima; Y. Honda; O. Kitao; H. Nakai; T. Vreven; K. Throssell; J. A. Montgomery Jr; J. E. Peralta; F. Ogliaro; M. J. Bearpark; J. J. Heyd; E. N. Brothers; K. N. Kudin; V. N. Staroverov; T. A. Keith; R. Kobayashi; J. Normand; K. Raghavachari; A. P. Rendell; J. C. Burant; S. S. Iyengar; J. Tomasi; M. Cossi; J. M. Millam; M. Klene; C. Adamo; R. Cammi; J. W. Ochterski; R. L. Martin; K. Morokuma; O. Farkas; J. B. Foresman and D. J. Fox, *Gaussian16, Revision C. 01*, Gaussian, Inc., Wallingford CT 2016.
33 M. Walker, A. J. A. Harvey, A. Sen and H. E. C. Dessent, Performance of M06, M06-2X, and M06-HF density functionals for conformationally flexible anionic clusters: M6 functionals perform better than B3LYP for a model system with dispersion and ionic hydrogen-bonding interactions, *J. Phys. Chem. A*, 2013, **117**(47), 12590–12600.
34 F. J. Stanton, Why CCSD(T) works: a different perspective, *Chem. Phys. Lett.*, 1997, **281**(1–3), 130–134.
35 D. R. Bell and K. A. Wilson, SO_3 revisited: Impact of tight d augmented correlation consistent basis sets on atomization energy and structure, *Chem. Phys. Lett.*, 2004, **394**(1–3), 105–109.
36 L. J. M. Marti, A fully *ab initio* quartic force field of spectroscopic quality for SO_3, *Spectrochim. Acta*, 1999, **55**(3), 709–718.
37 A. P. Denis, Basis set requirements for sulfur compounds in density functional theory: a comparison between correlation-consistent, polarized-consistent, and People-type basis sets, *J. Chem. Theory Comput.*, 2005, **1**(5), 900–907.
38 X. N. Wang and K. A. Wilson, Density functional theory and the correlation consistent basis sets: the tight *d* effect of HSO and HOS, *J. Phys. Chem. A*, 2005, **109**(32), 7187–7196.
39 P. B. Pritchard, D. Altarawy, B. Didier, D. T. Gibson and L. T. Windus, New Basis Set Exchange: an open, up-to-date resource for the molecular sciences community, *J. Chem. Inf. Model.*, 2019, **59**(11), 4814–4820.
40 J. T. Lee and R. P. Taylor, A diagnostic for determining the quality of single-reference electron correlation methods, *Int. J. Quantum Chem.*, 1989, **36**(S23), 199–207.
41 C. Gonzales and H. B. Schlegel, Reaction path following in mass-weighted internal coordinates, *J. Phys. Chem.*, 1990, **94**, 5523–5527.
42 I. M. Alecu, J. Zheng, Y. Zhao and D. G. Truhlar, Computational thermochemistry: scale factor databases and scale factors for vibrational frequencies obtained from electronic model chemistries, *J. Chem. Theory Comput.*, 2010, **6**, 2872–2887.
43 D. G. Truhlar, B. C. Garrett and S. J. Klippenstein, Current status of transition-state theory, *J. Phys. Chem.*, 1996, **100**(31), 12771–12800.
44 A. Miyoshi, *GPOP software, rev. 2022.01.20ml*, available from the author. See **http://akrmys.com/gpop/**.
45 R. L. Brown, A method of calculating tunneling corrections for Eckart potential barriers, *J. Res. Natl. Bur. Stand.*, 1997, **86**(4), 357–359.
46 A. M. Dean and H.-H. Carstensen, Chapter 4 The kinetics of pressure-dependent reactions, *Compr. Chem. Kinet.*, 2007, **42**, 101–184.
47 A. Miyoshi, *SSUMES software, rev. 2018.06.14m5*, available from the author. See **http://akrmys.com/ssumes/**.
48 J. Troe, Theory of thermal unimolecular reactions at low-pressures. I. Solutions of the master equation, *J. Chem. Phys.*, 1977, **66**, 4745–4757.
49 H. Hippler, J. Troe and H. J. Wendelken, Collisional deactivation of vibrationally highly excited polyatomic molecules. III. Direct observations for substituted cycloheptatrienes, *J. Chem. Phys.*, 1983, **78**, 6718–6724.
50 *GEOS-chem (GC Classic) 14.1.1*, DOI: **10.5281/zenodo.7696651**.
51 R. Gelaro, W. McCarty, M. J. Suárez, R. Todling, A. Molod, L. Takacs, C. A. Randles, A. Darmenov, M. G. Bosilovich, R. Reichle, K. Wargan, L. Coy, R. Cullather, C. Draper, S. Akella, V. Buchard, A. Conaty, A. M. da Silva, W. Gu, G.-K. Kim, R. Koster, R. Lucchesi, D. Merkova, J. E. Nielsen, G. Partyka, S. Pawson, W. Putman, M. Rienecker, S. D. Schubert, M. Sienkiewicz and B. Zhao, The Modern-Era Retrospective Analysis for Research and Applications, version 2 (MERRA-2), *J. Clim.*, 2017, **30**(14), 5419–5454.

52 E. E. McDuffie, S. J. Smith, P. O'Rourke, K. Tibrewal, C. Venkataraman, E. A. Marais, B. Zheng, M. Crippa, M. Brauer and R. V. Martin, A global anthropogenic emission inventory of atmospheric pollutants from sector- and fuel-specific sources (1970-2017): an application of the Community Emissions Data System (CEDS), *Earth Syst. Sci. Data*, 2020, **12**, 3413–3442.

53 G. Janssens-Maenhout, M. Crippa, D. Guizzardi, F. Dentener, M. Muntean, G. Pouliot, T. Keating, Q. Zhang, J. Kurokawa, R. Wankmüller, H. Denier van der Gon, J. J. P. Kuenen, Z. Klimont, G. Frost, S. Darras, B. Koffi and M. Li, HTAP_v2.2: a mosaic of regional and global emission grid maps for 2008 and 2010 to study hemispheric transport of air pollution, *Atmos. Chem. Phys.*, 2015, **15**, 11411–11432.

54 V. V. Pham, J. Tang, S. Alam, C. Lokan and H. A. Abbass, Aviation emission inventory development and analysis, *Environ. Model. Softw.*, 2010, **25**(12), 1738–1753.

55 G. R. van der Werf, J. T. Randerson, L. Giglio, T. T. van Leeuwen, Y. Chen, B. M. Rogers, M. Mu, M. J. E. van Marle, D. C. Morton, G. J. Collatz, R. J. Yokelson and P. S. Kasibhatla, Global fire emissions estimates during 1997–2016, *Earth Syst. Sci. Data*, 2017, **9**(2), 697–720.

56 A. B. Guenther, X. Jiang, C. L. Heald, T. Sakulyanontvittaya, T. Duhl, L. K. Emmons and X. Wang, The Model of Emissions of Gases and Aerosols from Nature version 2.1 (MEGAN2.1): an extended and updated framework for modeling biogenic emissions, *Geosci. Model Dev.*, 2012, **5**, 1471–1492.

57 J. Peeters, J. F. Müller, T. Stavrakou and V. S. Nguyen, Hydroxyl radical recycling in isoprene oxidation driven by hydrogen bonding and hydrogen tunneling: the upgraded LIM1 mechanism, *J. Phys. Chem. A*, 2014, **118**, 8625–8643.

58 G. Manonmani, L. Sandhiya and K. Senthilkumar, Reaction of Criegee Intermediates with SO_2 – A possible route for sulfurous acid formation in the atmosphere, *ACS Earth Space Chem.*, 2023, **7**(10), 1890–1904.

59 P. Pulay, A perspective on the CASPT2 method, *Int. J. Quantum Chem.*, 2011, **111**(13), 3273–3279.

60 S. Hattori, Y. Iizuka, B. Alexander, S. Ishino, K. Fujita, S. Zhai, T. Sherwen, N. Oshima, R. Uemura, A. Yamada, N. Suzuki, S. Matoba, A. Tsuruta, J. Savarino and N. Yoshida, Isotopic evidence for acidity-driven enhancement of sulfate formation after SO2 emission control, *Sci. Adv.*, 2021, **7**(19), eabd4610.